

Detection in Collision Avoidance Radar Using Active versus Passive Phased Arrays

Amir I. Zaghloul^{1,2}, Ron Wellman¹, and Theodore K. Anthony¹

¹US Army Research Laboratory, Adelphi, MD

²Virginia Polytechnic Institute and State University, VA

amir.zaghloul@us.army.mil, rwellman@arl.army.mil, tanthony@arl.army.mil

Abstract—This paper presents two designs for phased arrays for collision avoidance radar operating at the 76 GHz band. The two designs for the antenna use a linear waveguide horn array that is fed with a waveguide power-dividing network and is tapered to produce low side-lobe levels for low-error detection. The taper is based on a 40-dB Taylor distribution. The first design uses passive phased arrays that are stacked and bore-sighted in different directions to produce scanned beams through switching. The second design uses a single phased array with MEMS phase shifters embedded in the last stage of the waveguide power divider. The phase shifters are integrated with the help of MIC/MMIC-to-waveguide or waveguide-to-coplanar-waveguide (CPW) transitions that are housed in the waveguide sections that feed the array elements. The antenna and detection system measurement results of the passive array design are presented, along with the simulation results of the active array design.

1. INTRODUCTION

The phased array for the personnel collision avoidance radar system is designed to have the ability of detecting personnel at much larger range than their electro-optics counterpart, even in bad weather, thus providing the additional time necessary to control the vehicle. The performance requirements for the radar for which the antenna was designed were to have a minimum detection range of 150 m for an individual moving at 1 m/s with respect to the background [1]. In addition, the radar must be able to detect and follow a vehicle at a fixed range. The system requires continuously scanning antennas to be mounted on the vehicle with narrow beams in the azimuth (horizontal) direction and broad beam in the elevation (vertical) direction.

2. SYSTEM USING SWITCHABLE PASSIVE ARRAYS

A block diagram for the first design is shown in Figure 1. The transmit antenna is a simple pyramidal horn of dimensions $2.6\lambda \times 2.6\lambda$ with broad beams in both azimuth and elevation. The basic unit in the receive antenna is a linear array with a tapered aperture for side-lobe control, and is implemented with pyramidal horn elements with no active components for beam control. The linear horn array design produces a 2-degree narrow beam in azimuth and a

broad 30-degree beam in elevation. Two groups of eight arrays that are stacked vertically with an azimuth tilt of 2 degrees between adjacent antennas cover a scanning range of ± 15 degrees. The beam is switched in azimuth using a microwave switch connected to the outputs of the antennas.

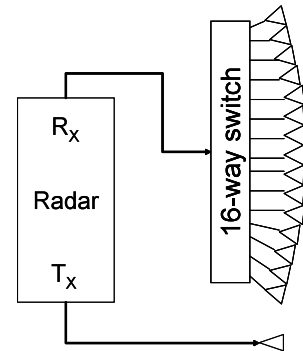


Figure 1. Block diagram

The receive antenna array is composed of 32-elements fed with a waveguide power divider designed to produce a 33dB Taylor distribution across the array aperture [2], [3]. The overall configuration is shown in Figure 2, and measures 0.5" (height) X 7.0" (width) X 5.0" (depth). The horns are 1.3λ in the H-plane (array plane) and 2.0λ in the E-plane. The 5-stage H-plane waveguide power divider uses un-equal power splits in the 2nd through the 4th stages to achieve the required aperture distribution. The first and last stages use equal-split power dividers with a fourth port with a short-circuit termination to improve the impedance match. The equal power division in the 5th stage of the power divider represents a compromise that is needed due to the tight dimensions that are dictated by the element spacing. This resulted in a closer low-level grating lobe, in addition to the higher level grating lobes at ± 50 degrees that result from the 1.3λ horn dimension. This, however, does not compromise the side-lobe requirement within the operating scanning range of ± 15 degrees that is needed for the collision avoidance system. Detailed analysis and HFSS simulations of the design and power divider matching are included in [2] and [3] with the fabrication, measurements and characterization of the antenna. Figures 3-5 display HFSS's simulations of the E-fields in the 50/50 split, 93/07 split and the symmetrical half of the array with the Taylor distribution, respectively.

The antenna design shown in Figure 2 was fabricated as a fully integrated horn array and 5-stage power divider. The structure was milled in two pieces using numerical control techniques with very tight tolerances. The fabricated antenna is shown in Figure 6. The two pieces of the fabricated antenna are almost identical. The 4th ports in the first and last stages of the power divider are added to one of the two pieces. This was implemented by milling a hole through and then inserting a piece from the outside of the structure to act as a short stub. Again, tight tolerances have to be exercised in order to satisfy the RF boundary conditions. The assembly of the transmit horn and the 16 passive receive arrays for the 16 switchable beam positions is shown in Figure 7.

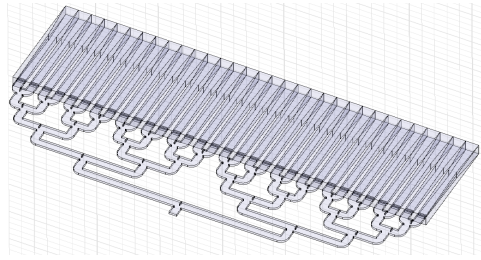


Figure 2. Horn array configuration with feeding waveguide power dividing network

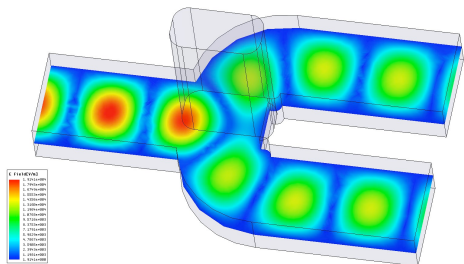


Figure 3. Simulation of 50/50 power split

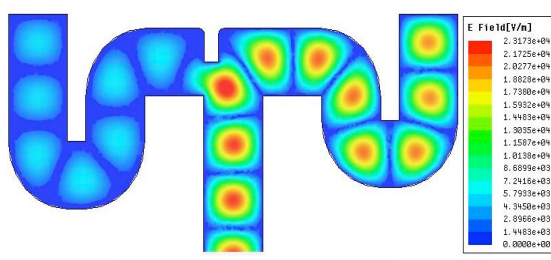


Figure 4. Power split of 93/07

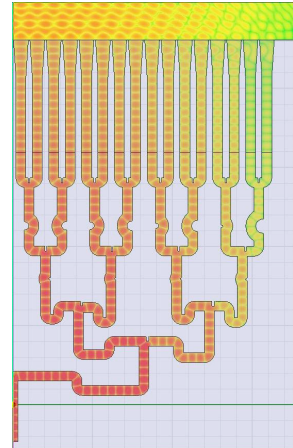


Figure 5. Array half with Taylor distribution

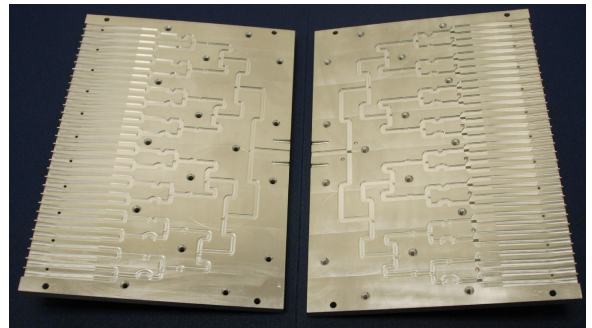


Figure 6. Fabricated passive array

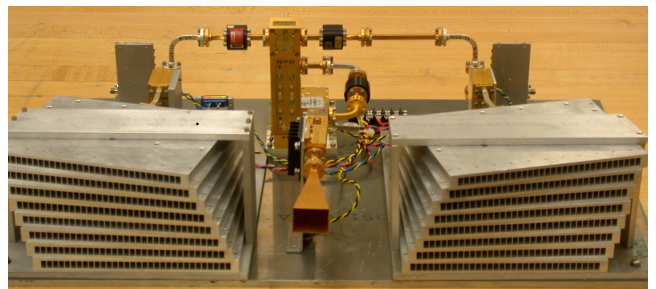


Figure 7. Assembly of transmit and receive antennas

The fabricated receive antenna was measured at the operating bandwidth around 76GHz. The measurements included return loss, radiation patterns and gain. Measured results agreed with the HFSS simulation. The radiation pattern, measured at different frequencies, is shown in Figure 8. High-level grating lobes appear close to 50 degrees from boresight and caused by the 1.3λ element spacing. Lower-level grating lobes appear closer in, and are

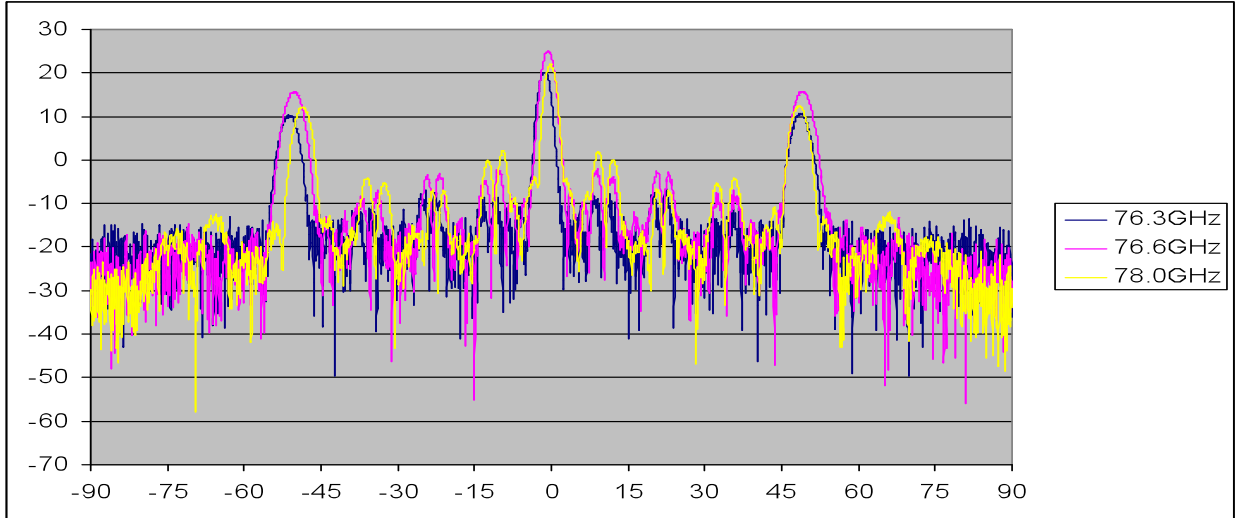


Figure 8. Measured radiation patterns

caused by the equal split power division in the last stage of the power divider, resulting in a periodic spacing of 2.6λ .

The collision avoidance radar system using the passive receive arrays was tested in real environments. The detection of moving targets from a moving platform is limited by clutter spread in Doppler domain. This spread is caused by the subtended beam angle of the clutter and the vehicle motion. For example, the clutter line, with a 2-degree beam pointing at 15 degrees from forward for a vehicle traveling at 10 m/s has a velocity spread from 9.61 to 9.74 m/s. The detection of slow moving targets is limited by this spread. Since the receive antenna has a high-level grating lobe at 50 degrees, there is another clutter line covering velocities from 6.2 to 6.7 m/s that could limit detection or create false targets. This effect would be most noticeable when buildings are present on the side of the road. This problem is evident in Figure 9. This data is from a W-band radar moving down the road with a person walking along the side of the road. The large numbers of detections from 15 to 40 m are caused by the receive antenna grating lobes. These could be reduced with tracker modifications or virtually eliminated with an antenna redesign. This leads to the second design that uses active phased arrays for transmit and receive antennas.

3. ACTIVE ARRAY PERFORMANCE

The second design uses an active array for both transmit and receive antennas. A single receive array replaces the 16 passive arrays. Four-bit MEMS phase shifters are inserted in the last stage of the waveguide power divider. The phase shifters are integrated on microstrip lines that are inserted in the feeding waveguides using waveguide-to-microstrip or waveguide-to-coplanar waveguide transition, discussed in the next section. The transmit antenna uses a similar active array that produces a narrow transmit beam. Using the same array design for the transmit and receive antennas improves the effective side-lobe and grating lobe performances in the

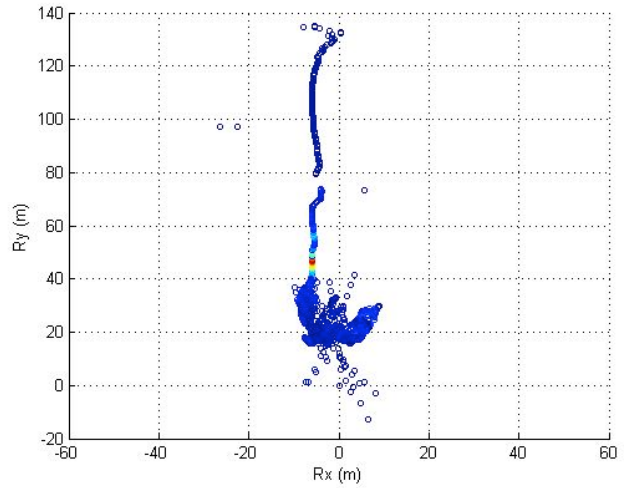


Figure 9. Field test data of moving targets using the high-level grating lobe receive arrays

system. This alleviates the clutter problem caused by the high grating lobe level observed in the passive receive array/single transmit horn design.

Examples of the radiation patterns of scanned beams are shown in Figure 10 for 0° , $\pm 5^\circ$, and $\pm 15^\circ$ beams. The figure shows the patterns when ideal phase shifts are imposed on the signals in the different array elements to produce the scanned beams. In the realization of the system, multiple-bit phase shifters are used, which quantize the values of the phase shifts to the next bit. The beam is scanned through switching the states of the phase shifter bits using fast MEMS switches. Figure 11 shows the same patterns in the 0° , $\pm 5^\circ$, and $\pm 15^\circ$ directions when 4-bit phase shifters are used. This quantizes the phase shift values to steps of 22.5° . The effects of the quantization are evident in increasing side-lobe levels.

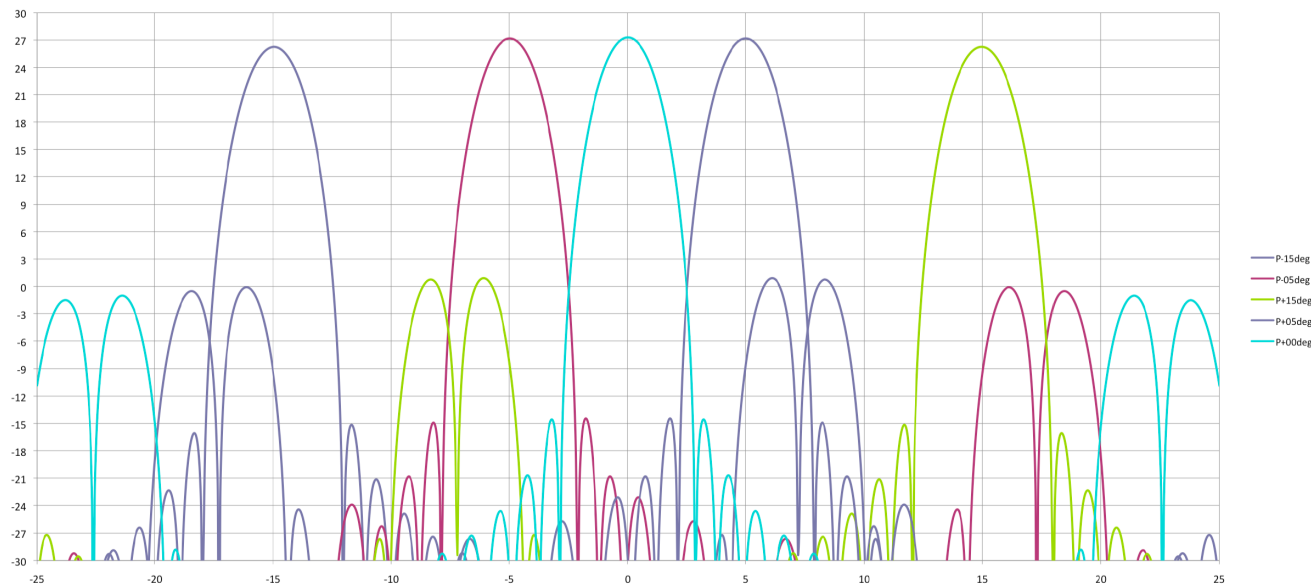


Figure 10. Radiation patterns for beams scanned at 0° , $\pm 5^\circ$, $\pm 15^\circ$ with ideal phase shifters

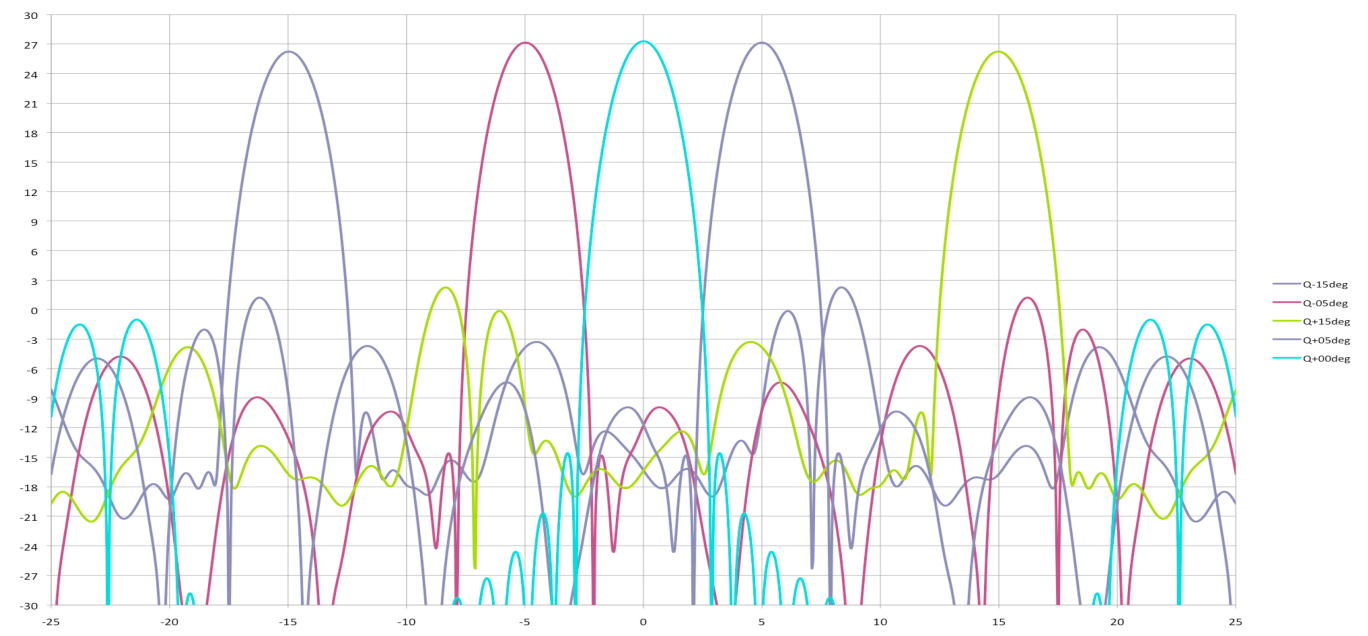


Figure 11. Radiation patterns for beams scanned at 0° , $\pm 5^\circ$, $\pm 15^\circ$ with quantized, 4-bit phase shifters

4. PHASE SHIFTER INTEGRATION

The waveguide structure of the power dividing network was selected to reduce the losses, which is a key requirement for receive antennas. In the active array design, the 16 arrays are replaced with a single array that employs phase shifters embedded in the waveguide power divider, which are used for fast beam steering. The power divider still uses the waveguide as a low-loss medium. The integration of the phase shifters in the waveguide power-dividing network requires a low-loss transition between the waveguide and the phase shifter implementation medium. Two implementation media have been used extensively, MMIC and MEMS. The MMICs have a mature process, high yield and provide fast switching. However, their losses may be too high for receive applications. The MEMS, on the other hand, are less mature, their reliability criteria are not well established and may have limitations on their switching speeds. However, they offer lower losses than their MMIC counterparts. The MEMS phase shifters can use MIC transmission lines as their integration vehicle in the power dividing structure. They can also be integrated using co-planar waveguides, resulting in lower losses.

A microstrip-to-waveguide transition for the integration of the MEMS phase shifters in the waveguide power-dividing network is shown in Figure 12 [4]. The MEMS phase shifter will replace the MIC or MMIC circuit in the figure. The transition shown in Figure 12 was designed for Ka-band operation around 20 GHz. The insertion loss and return loss of the back-to-back transitions are shown in Figure 13. The insertion loss of the transition, including the losses in the MIC line is around 1 dB in the 19-20 GHz region. Losses at the higher frequencies around 76 GHz will be higher. Additional losses will be incurred in the transition to the MEMS phase shifter that is mounted on the MIC circuit. These losses may be extensive for the receive array operation.

A more efficient medium for the integration of the MEMS phase shifter is the co-planar waveguide (CPW). It has less loss relative to the microstrip medium. The presence of the ground plane on the same side as the active line makes the integration of electronic circuits simpler with coplanar bias and control lines. A waveguide-to-co-planar-waveguide transition facilitates the insertion of the MEMS phase shifters in the waveguide power dividing network of the phased array.

The waveguide-to-CPW transition, sketched in Figure 14, is a dielectric septum of small thickness with a tapered metallization on one side [5]. The center portion of the transition accommodates the CPW circuit and its length is determined accordingly. The center conductor of the CPW extends through the whole length of the transition. This creates a CPW with a decreasing width of the slot between the center conductor and the co-planar ground planes to

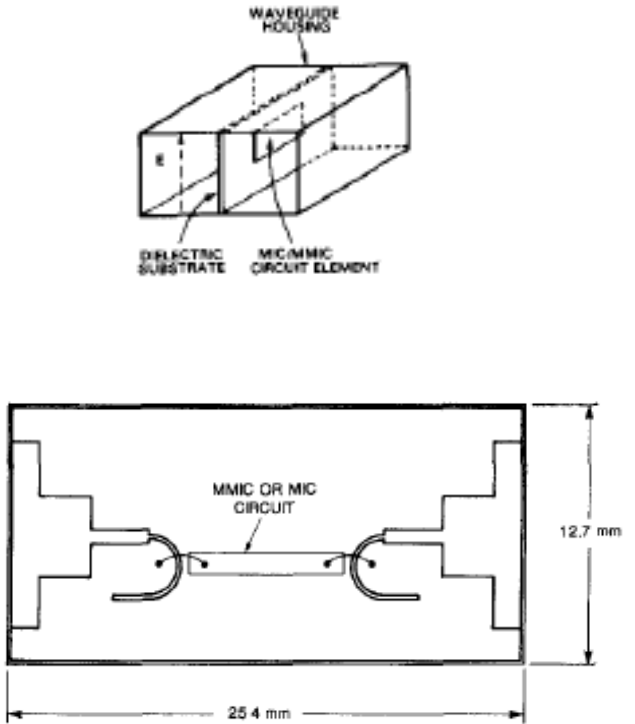


Figure 12. Microstrip-to-waveguide transition for phase shifter insertion in waveguide feed network

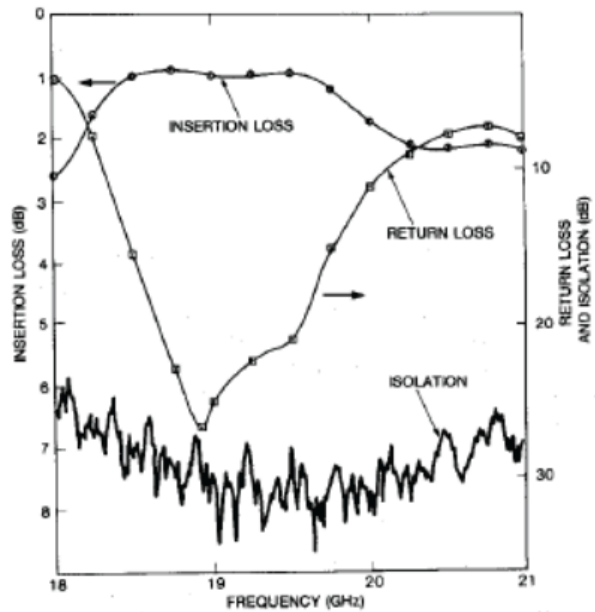


Figure 13. Measured performance of microstrip-to-waveguide transition fabricated at Ka-band

produce the match across the frequency band. Two rectangular openings in the top and bottom walls of the waveguide provide mechanisms for biasing the components that are mounted on the CPW. The surface current distribution along the transition is shown in Figure 15.

Using equally spaced multiple septa with the same tapered metallization on both sides of the active transition, i.e. the center septum with the CPW, produces lower insertion loss and a better match across a portion of the frequency band. The structure of a 7-septa transition is shown in Figure 16.

The waveguide-to-CPW transition was simulated using the full-wave analysis tool HFSS. The S parameters (insertion and return losses) were calculated with a waveguide input, followed by the transition that goes back to a waveguide output. A WR-12 rectangular waveguide was assumed in the simulation. The results are shown in Figure 17 for five cases, ranging from a waveguide with un-metallized dielectric septum with no openings on the top and bottom walls of the waveguide to a 7-septa transition. The results show the broadband operation of the transition, covering a band of 60 to 100 GHz, and zoomed over the 72-75 GHz band, with good insertion and return losses. The 7-septa transition shows better results within the bandwidth of 72-75 GHz.

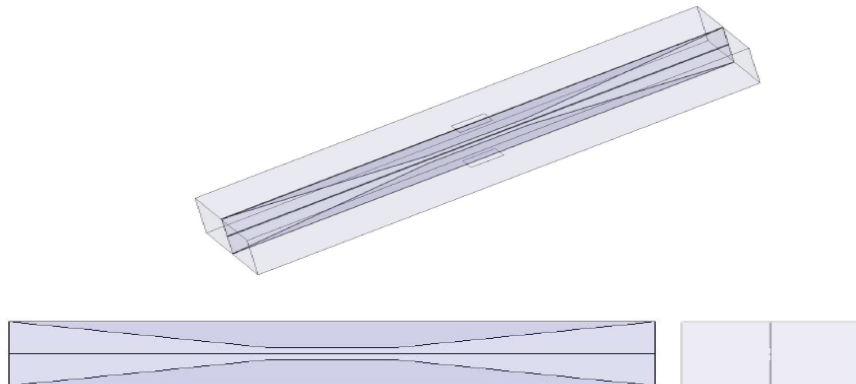


Figure 14. Waveguide-to-CPW transition with a single septum shown in isometric view and front and side projections

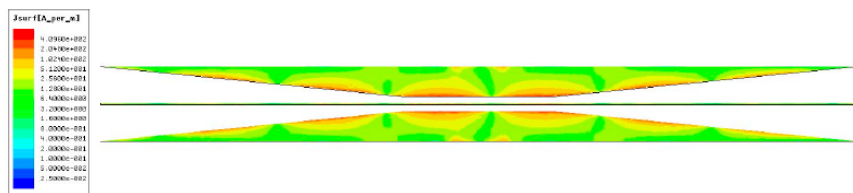


Figure 15. Surface current distribution in the waveguide-to-CPW transition

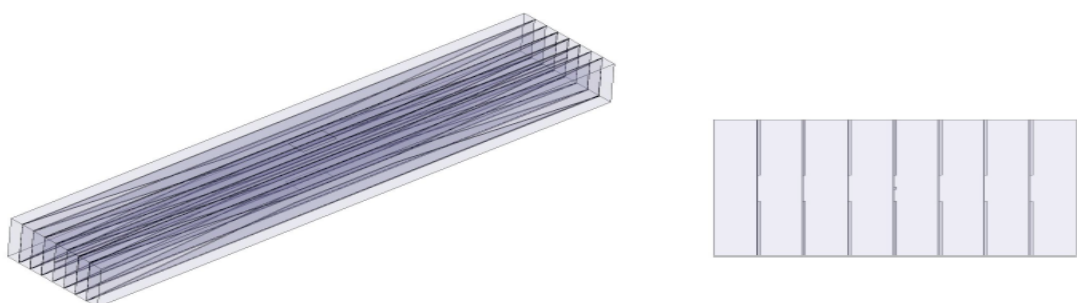


Figure 16. Waveguide-to-CPW transition with seven septa shown in isometric view and front projection, indicating the CPW on the center septum only

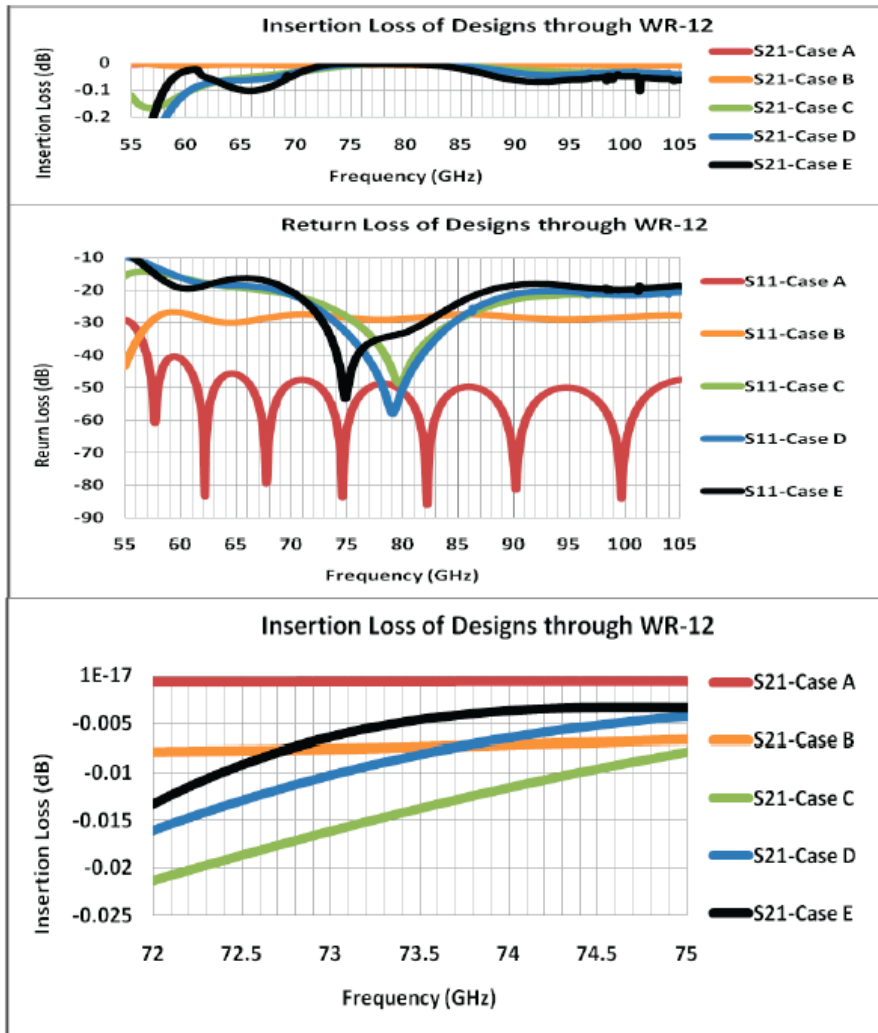


Figure 17. Insertion loss and return loss for different configurations of waveguide-to-CPW transition in comparison with dielectric septum with no metallization in the waveguide

Case A- A 15mm long section of 0.25 mil thick substrate of Cuflon with no metallization inserted into WR12 waveguide without top & bottom holes.

Case B- A 15mm long section of 0.25 mil thick substrate of Cuflon with no metallization inserted into WR12 waveguide with top & bottom holes.

Case C- A 15mm long section of 0.25 mil thick substrate of Cuflon with tapered metallization transition inserted into WR12 waveguide with top & bottom holes.

Case D- Three equally spaced 15mm long sections of 0.25 mil thick substrate of Cuflon with tapered metallization transition inserted into WR12 waveguide with top & bottom holes.

Case E- Seven equally spaced 15mm long sections of 0.25 mil thick substrate of Cuflon with tapered metallization transition inserted into WR12 waveguide with top & bottom holes.

The insertion loss of the waveguide-to-CPW is a fraction of the corresponding insertion loss of the waveguide-to-MIC/MMIC. This makes the CPW and its transition in the waveguide medium of the array's power divider network a better choice that also offers a simpler integration medium.

5. CONCLUSION

The linear array of pyramidal horns fed with a waveguide power divider is an efficient design for the personnel collision avoidance radar system. 16 passive arrays, designed with a Taylor aperture distribution give the required side-lobe level for a boresight beam. Stacking the 16 arrays with shifted boresight directions produce the required scanning directions within the coverage angle. Using a single active array instead, can produce the 16 beam directions that are generated using MEMS phase shifters that are inserted in the waveguide feed array. Waveguide-to-MIC/MMIC transitions can be used to integrate the phase shifters in the waveguide power-dividing network. A lower-loss solution is to use a waveguide-to-CPW transition for the same purpose and for easier integration. A septum-type transition couples energy with very low loss over a broad bandwidth from the waveguide into the CPW circuit. This transition is virtually lossless with a bandwidth greater than 50%. It provides a single-piece, rugged module that is easily and inexpensively produced. A multiple-septa design showed lower insertion loss over around a 4% bandwidth.

REFERENCES

- [1] R. Wellman, E. Adler, M. Conn, A. Zaghloul, T. Anthony, and S. Schmidt, "Advanced Perception Radar for Large Robotic Vehicles," MSS Tri-Service Radar Symposium, Boulder, Colorado, June 2009.
- [2] A. Zaghloul and T. Anthony, "A 76-GHz Antenna with Highly-Tapered Aperture for Collision Avoidance System," *Invited Paper*, European Conference on Antennas and Propagation (EuCAP), March 2009.
- [3] T. Anthony and A.I. Zaghloul, "Designing a 32 Element Array at 76 GHz with a 33 dB Taylor Distribution in Waveguide for a Radar System," IEEE International Symposium on Antennas and Propagation, Charleston, South Carolina, June 2009.
- [4] B. D. Geller and A. I. Zaghloul, "An MMIC/MIC-to-Waveguide Transition for Single- and Dual-Polarization Systems," IEEE MTT-S Digest, 1984, pp. 412-413.
- [5] T.K. Anthony and A.I. Zaghloul, "Waveguide-to-CPW Transition for an Active Phased Array for Collision Avoidance Radar," IEEE International Conference on Wireless Information Technology and Systems, Honolulu, Hawaii, August-September 2010.